Journal of Magnetism and Magnetic Materials 118 (1993) 248–262
North-Holland

NMR measurements on obliquely evaporated Co–Cr films

J.C. Lodder [a], H. van Kranenburg [a], K. Takei [b] and Y. Maeda [b]

[a] *MESA Research Institute, University of Twente, P.O. Box 217, 7500 AE Enschede, The Netherlands*
[b] *NTT Basic Research Laboratories, Material Science Research Laboratory, Tokai, Ibaraki 319-11, Japan*

Received 6 January 1992

The distribution of the hyperfine fields or the resonance frequencies in metals and alloys obtained by NMR measurements have been known for a long time. Recently, new experimental data have been published about thin films for studying their chemical inhomogeneities. An example is the study on sputtered and evaporated Co–Cr layers. In this paper we report on the compositional distribution of co-evaporated Co–Cr films by using the Co spin-echo NMR technique. For comparison single source evaporated samples of Co–Cr and pure Co as well as two alloyed ribbons ("bulk" samples) have also been measured. Based on the NMR results the local Cr concentration of the ferromagnetic and less ferromagnetic regions are determined. In comparison the data from the co-evaporated films, even at low substrate temperature, have clearly shown the presence of a process-induced compositional separation. This is in qualitative agreement with the magnetic properties of the samples.

1. Introduction

Sputtered Co–Cr films for perpendicular recording were first mentioned by Iwasaki et al. in 1975 [1]. Although in the meantime many alternative materials have been proposed, Co–Cr is still the medium mostly used for application in perpendicular recording. During recent years deposited (sputtered and evaporated) Co–Cr media have been improved in many aspects and many good results have been reported on their practical use [2].

The basic magnetic properties such as magnetization, coercivity and anisotropy depend on microstructural properties, compositional separation of Co and Cr and phase separation. These inhomogeneities are the main source for the deviation of the saturation magnetisation (M_s) from the Slater–Pauling curve (see below) which gives the relation between the saturation magnetization (M_s) and homogeneous bulk Co–Cr [3].

In general most papers reported that the M_s of sputtered and evaporated films, deposited at higher substrate temperatures, is found to be larger than that for bulk alloys having the same average chemical composition. Although in the literature various origins have been proposed the most likely explanation is the phase separation. Two hcp phases, which hardly occur in bulk Co–Cr material at low temperatures, cause compositional fluctuations along the grain boundaries as the film growth proceeds. In ref. [35] it was explained that the separation into a ferromagnetic and paramagnetic (ε-Co) phases appears to be the most likely explanation. With a non-homogeneous distribution of Cr in the Co the 3d shells of Co stay unfilled. Consequently this gives rise to a high magnetic moment. The Cr-rich areas with a Cr content higher than 25 at% are non-ferromagnetic and are too small to compensate for this high M_s. As a result, the average value of M_s for a Co–Cr film with a compositional separation becomes higher.

Correspondence to: Dr. J.C. Lodder, MESA Research Institute, University of Twente, P.O. Box 217, 7500 AE Enschede, The Netherlands. Tel.: +31-53-899111.

Very frequently such a compositional inhomogeneity shows the so-called CP structure [8–12] within the Co–Cr grains. In such layers the compositional fluctuation have been clearly demonstrated by a selective chemical etching method (e.g. ref. [8]). Very recently NMR studies of such compositional inhomogeneities in sputtered Co–Cr have been published [13] and the results are consistent with the model of compositional separation as mentioned above.

Two different types of thin obliquely evaporated Co–Cr films have been prepared. In one type the deposition of Co–Cr was made from one alloyed source and in the other type co-evaporated films were made in which two vapour beams being directed from opposite directions, one source containing Co and the other Cr. Shadowing effects during deposition play an important role in the nucleation and growth of the layers. In the case of the co-evaporated method the geometry of the deposition induces separated regions that are Co- and Cr-rich. Consequently this enables us to deposit Co–Cr films consisting of a so-called process-induced compositional separation which shows enhanced perpendicular magnetic properties, even at low substrate temperatures [4–7]. This is in contrast with sputtered Co–Cr films which have always been deposited at elevated substrate temperatures in order to obtain the necessary magnetic properties which are in general caused by the pronounced compositionally separated state of the samples. It has been shown for sputtered films that a compositionally modulated structure of ferromagnetic Co-rich and less-ferromagnetic Cr-rich phases appears [8].

An alternative method for preparing Co–Cr films for high density recording is evaporation [14], using a continuous roll-coater deposition. Again in this type of film a spatial distribution of Co and Cr has also been measured. It has been shown by NMR and TEM in combination with selective etching [14,15] that the compositional distribution is shown in a CP structure.

In the above-mentioned research on evaporated and sputtered layers, NMR has shown to be a very useful tool for determining the various compositions of thin Co–Cr films.

1.1. NMR measurements

Applying the NMR technique very precise measurements are possible of the distribution of the hyperfine fields or the resonance frequencies in metals and alloys.

Hyperfine interactions (interactions between electrons and nucleus) have been studied since Pauli's postulation on the existence of a spin-angular momentum and an associated magnetic nucleus moment [16]. The magnetic hyperfine interaction was first given by Fermi using the Dirac relativistic theory for the electron. Later this theory was extended for multi-electron contributions to the hyperfine interactions. One of the well-know experimental techniques for studying the hyperfine interactions is the application of the Mössbauer effect. This method can be used for many applications because it does not make use of an rf field, which is needed in the NMR technique. Due to the fact that the energy associated with the nucleus–electron interaction is very much smaller than that needed for electron–electron interaction in ordered magnetic materials a simplification in the theoretical approach as proposed by ref. [17] is permitted. Here the nuclear energy may then be written as:

$$E = m\mu_n H_n / I,$$

where m is the magnetic quantum number of the nucleus, μ_n is the nuclear moment, I is the nuclear spin and H_n is the field established by the electron magnetization.

Nuclear resonance can be obtained when the quantum energy in the rf field $h\nu = \Delta E$. Here ΔE is the energy splitting ($= \mu_n H_n / I$).

The transition probability can be calculated from the resonance theory and it is found that for a resonance of ^{59}Co the fractional energy absorption should be about 10^{-5}. Experimentally an enormous enhancement is found in relation to the computed value namely 5 orders of magnitude greater. The reason for the enhancement is that the resonance is not driven by the external rf field directly (from the coils used around the sample) but indirectly by the nuclear–electron hyperfine coupling. The effect of a transverse rf

field within the limit that the electron and nuclear spins are decoupled is to turn the electron magnetization M through an angle H_x/H_a, whereby H_x is the external rf field and H_a the static anisotropy field acting on the electrons. The transverse magnetization than will be $M_x = MH_x/H_a$. The nucleus then experiences a transverse field [18]:

$$2H_1 = H_x + (M_x/M)H_n = (1 + H_n/H_a)H_x.$$

The transition probability, and thus the absorption rate, will then be enhanced by the factor $(1 + H_n/H_a)^2$. In the case of pure Co fcc, H_n is 215 kOe and $H_a = 1$ kOe which gives an enhancement factor of 4.7×10^4.

It can be concluded from this that nuclear resonance excitation in ferromagnetic materials takes place indirectly from the sample magnetization.

Associated magnetic moments of the spins of the nuclei are measured by the unit of the nuclear magneton, which is given by:

$$M_n = \mu_0 eh/2m_p = 6.33 \times 10^{-33} \text{ Wbm}.$$

Here M_n is the nuclear magneton, m_p is the mass of the proton and h is Planck's constant. The magnetic moment M/M for ^{59}Co is 4.460. The hyperfine-field H_n (kA/m) can be roughly approached by the following equation:

$$f = g(M_n/h)H_n = 1.24 \times 10^{-2} H_n.$$

In which f is the resonance frequency (MHz), g is the g-factor which has a value 1.31 for pure Co. Using the above-mentioned formulae we can calculate the hyperfine fields and in the case of Co the measured frequencies have about the same value as the calculated hyperfine fields. In general for ^{59}Co nuclei in fcc Co a frequency of 217 MHz and for hcp Co 220–228 MHz has been measured. The exact frequency depends on the crystal structure, morphology and chemical inhomogeneity. These frequencies are roughly in agreement, respectively, with hyperfine fields of 215 and 218–226 kOe, measured at 4 K.

In conclusion the hyperfine fields and thus the echo frequencies and their peak widths depend on many factors such as: crystallographic structure, chemical inhomogeneities, crystal faults, the average magnetization (proportionally) and stress. All those factors make it clear that we have to be careful with the interpretation of measured spectra of practical samples from which only a few of these aspects are known in general.

1.2. NMR experimental conditions

In this study a ^{59}Co NMR spin echo equipment, developed at NTT [21], was used in which a variable frequency spin-echo pulse at liquid-helium temperature was measured. The amplitude was detected as a function of the frequency which was directly related to the local hyperfine field of the material. All measurements were carried out at zero external field. The principle of the measurement is the creation of two sequential pulses of rf excitation to the material and measuring the spin echo amplitude as a function of the resonance frequency. The rf pulse width was 1 μs and the separation between the two pulses 15 μs. The applied rf field is less than about 25 Oe and depends on the size and shape of the measurement rf coil around the sample. Keeping the width and separation of the pulse constant the maximum echo was adjusted by the pulse amplitude. The echo intensity was plotted vs. the measured frequency f. In order to correct the echo intensity for the enhancement and Boltzmann factors [22] it is divided by f^2. In order to improve the reproducibility of the frequency measurement, the impedance mismatching in the transmission line of the equipment was decreased by connecting two 6 dB attenuators to the in and output connections of the sample holder.

1.3. The use of standard samples

The keypoint in the interpretation of NMR data is the use of standard samples to characterize the various NMR spectra. In most cases powder samples are used as references for the interpretation of the spectra measured from alloys, because these samples are much closer to the equilibrium state and their atoms are expected to be more uniformly distributed than in the case of

the deposited (Co–Cr) alloy films. The spin-echo frequencies of powdered Co–Cr [13,15], sputtered [13] and evaporated Co films as well as data for fcc [23] and hcp [19,20] Co-bulk materials are presented in fig. 1 as a function of the average at% Cr. It can be concluded from this figure that for a pure Co material the main echo frequency can be varied between 217 and 226 MHz. This is due to various reasons, namely the preparation method, purity, morphology and microstructure.

In binary hcp Co alloyed polycrystalline samples it was shown by ref. [20] that NMR spectra at 4.2 K for each alloy consists of a main line and satellite lines. A main line and satellite lines are also found in Co-alloys having an fcc structure and measured at 77 K [24]. The origin of these lines has been discussed by ref. [25]. The origin of the main line in powdered hcp Co (228 MHz at 0 K) was first described by ref. [26] as originating from the resonance coming from the nuclei in the domain wall. In single-crystal specimens [19] and polycrystalline samples [20] of hcp Co a domain-wall resonance frequency of about 225.5 MHz and a domain frequency of 220.5 MHz were reported.

The peak frequency and the peak width of the various Co alloy samples mentioned in the literature is rather complicated to understand since there are additional signals originating from mixed phase and fault structures [27,28], aging effects [29], deforming of Co-powders [30] and pressure dependence [31].

The influence of impurity atoms, Cr in this study, on the echo frequency is very important. A model is chosen based on an asumption that Cr is only situated as a completely isolated atom and the hyperfine fields are not affected by the impurities located further than the nearest neighbours (NN). Cr supplies a large number of electrons in the 3d band of the Co host material which leads to a redistribution of electrons in the NN sites of the Co atoms around the Cr. The moments of these Co-atoms surrounded by Cr are smaller than those from the isolated Co [24].

Powdered samples have been used up to now for calibrating the Co–Cr deposited films. The experimental data of this type of sample given in refs. [13,15,24], consisting of 0.6–22 at% Cr, have shown the same tendency for the peak profiles although there are remarkable differences. In

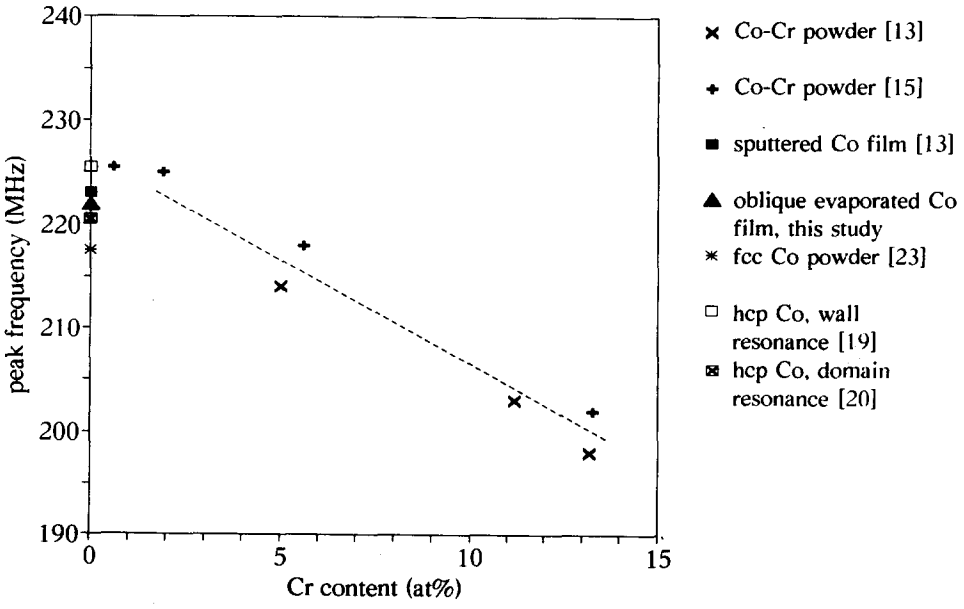

Fig. 1. The dependence of the main-line echo-peak frequency of the Cr concentration for various standard samples.

general (see fig. 2) a slightly diluted Co alloy consists of a main line and satellites.

The origin of the main line is from the Co nuclei without any Cr NN. The first satellite line appears at about 177 MHz and is caused by Co nuclei that have one Cr atom at their NN site. This satellite peak already occurs at an average at% Cr of about 1–2%. When the Cr at% increases to about 5% a second satellite peak appears at a frequency of about 130 MHz. In this case 2 Cr atoms are acting at the NN site of Co nuclei. The third satellite line which appears at about 11 at% Cr arises from three NN Cr atoms around the Co nuclei. In the case of Co–Cr the frequency intervals between the satellites and the main line is about equal to 40 MHz.

It is also shown that the main-line intensity and position change due to the increasing percentage of Cr. The effect of an increasing Cr amount becomes visible in the appearance of satellite peaks and a lower intensity of the main peak. Further, the main peak shifts slightly to smaller frequency and its width becomes larger (see also section 4). At 13% Cr even the first satellite can become higher in intensity than the main line. At 22 at% Cr the spectrum becomes very broad with its maximum at about 80 MHz. In the last case the individual main and satellite lines cannot be distinguished due to the overlap.

2. Co–Cr phase diagram

There has been much literature published on the Co–Cr binary phase diagram; the most important ones for so far being the diagrams of Elsea [32], Grigor'ev [33] and Alibert [34]. Recently a complete overview and new data were published by Ishida and Nishizawa [35].

With respect to the application of Co–Cr as thin-film media for magnetic recording the most interesting area of the phase diagram is around the temperature range from room temperature to 1000°C. Furthermore the compositional area of

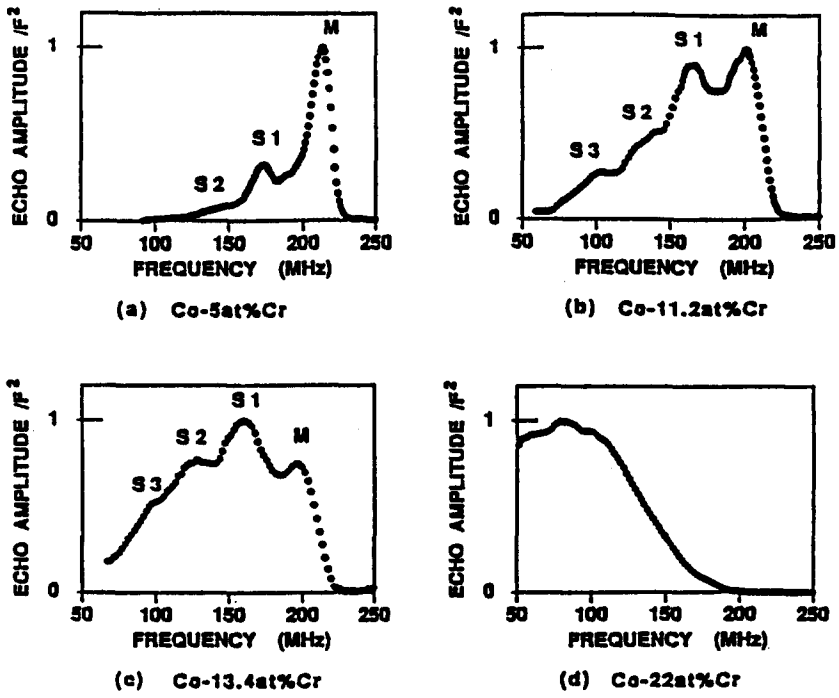

Fig. 2. Spin-echo spectra of powdered Co–Cr samples having various compositions [13].

interest is ≤ 35 at% Cr. In this part of the diagram two phases, α-fcc and ϵ-hcp are represented.

It can be seen from the latest published phase diagram [35] that even at 35 at% Cr a hcp ϵ-Co can exist (see fig. 3). There can be two phases, one with a high Co-rich composition (ferromagnetic) and the other with a high Cr-rich content (paramagnetic). The phase diagrams are based on an equilibrium process and achieved from thermodynamical calculations. The thin-film materials discussed here are made by deposition which is by definition a non-equilibrium process. In this case a very important fact was assumed in ref. [35], namely the phase diagram at high Co concentration below 800°C is very complicated because sluggish diffusion inhibits the equilibrium. It is known, for instance, that during sputtering the surface temperature of a grown film is quite different from that of the substrate [36]. The bombardment exerted by various particles from the plasma on the surface results in a much higher temperature at the surface. This and also the increase of substrate temperatures, ion-assisted deposition and geometrical deposition effects can stimulate the compositional inhomogeneity state of the thin film.

3. Various preparation techniques used in this study

In order to make a comparison we have measured pure Co and Co–Cr obliquely evaporated films, Co–Cr co-evaporated films and alloyed ribbons having two different compositions.

3.1. Evaporated films (single source)

At a pressure of 10^{-7} Torr a small amount of $Co_{80}Cr_{20}$ was evaporated by one e-gun on a Si substrate. As a function of time various samples have been deposited which resulted in a series with a variation of the composition of 13–31 at% Cr (due to the higher evaporation rate of Cr from the alloy source). The deposition was mostly car-

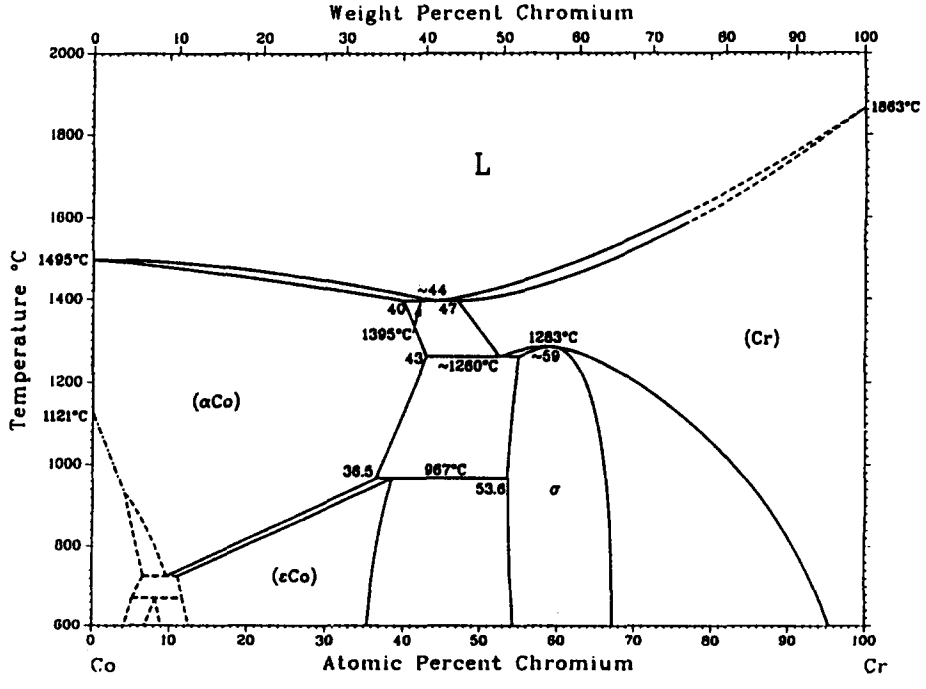

Fig. 3. Co–Cr phase diagram with the equilibrium phases: L = liquid; α-Co = fcc solid solution; ϵ-Co = hcp solid solution; Cr = bcc solid solution and σ = intermetallic phase [35].

Table 1
Properties of the obliquely evaporated Co–Cr films from one source

Sample	Subs. temp. [°]	at% Cr (XRF)	Thick-ness [nm]	M_s [kA/m]	$H_{c\perp}$ [kA/m]
M910423D	400	25.6	207	458	35
M910501E	RT	13.2	186	834	27
M910506E	RT	17.8	227	594	22
M910503E	RT	30.9	213	160	9

Table 2
Properties of obliquely co-evaporated Co–Cr films

Sample	Subs. temp. [°C]	at% Cr (XRF)	Thick-ness [nm]	M_s [kA/m]	$H_{c\perp}$ [kA/m]
M900712E	RT	24.7	356	471	57
M900713E	RT	21.5	648	540	49
M900718E	399	27.6	399	457	91
M900720E	400	27.3	753	498	92

ried out at RT but in one case at $T_p = 400$°C. The layer thickness varied from 180 to 230 nm and the angle of incidence was $\alpha_i = 27.5°$. Their magnetic parameters show a wide variation (see table 1). From XRD it can been concluded that all samples consist of a hcp phase. The samples prepared at 400°C have slightly higher d_{002} values than the RT samples.

3.2. Co-evaporated Co-Cr layers

The deposition was carried out in the same high vacuum system as mentioned above but in this case we used two e-beam sources. The angle of incidence, defined as the angle between the vapour flux and film normal was 27.5° for both Cr and Co vapour. The substrate was located in the common evaporation plane (defined by the two vapour-flux directions). Two deposition temperatures were used, namely ambient temperature and at 400°C. Heating of the substrate was carried out by infrared radiation and caused a process temperature (T_p) as mentioned.

The layer thicknesses we have investigated were 400 and 700 nm. The deposition rate was 0.4 nm/s. The average Cr content, determined by XRF, was measured from 22–28 at%. For further information please refer to table 2. All films show

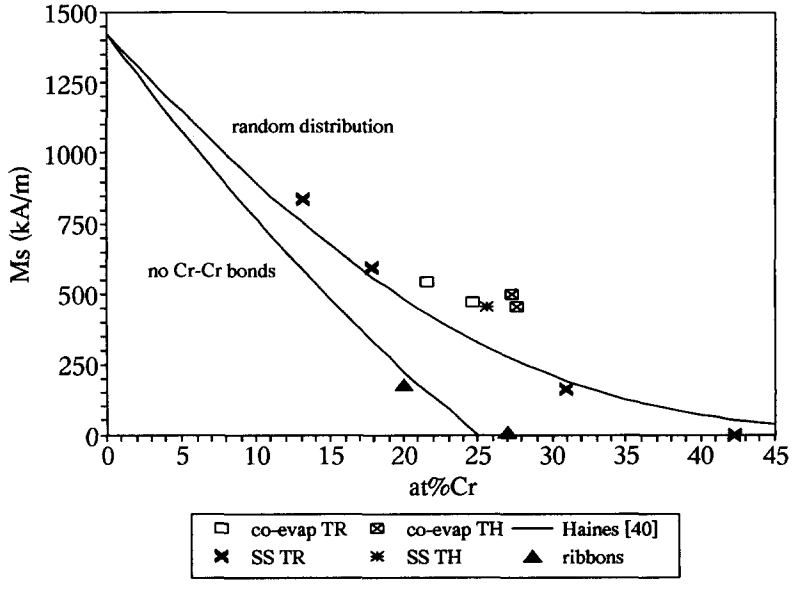

Fig. 4. Saturation magnetization vs. the average Cr content for different distributions of Cr in a Co hcp structure. No Cr–Cr bonds, random distribution and the studied samples.

a columnar morphology inclined towards the direction of the Co source. The angle depends on the substrate temperature and is 14–15° for the ambient temperature and 8–10° at 400°C. From XRD measurements it can be concluded that all films have the hcp structure. As for the one source samples we have observed the same tendency namely the HT samples have larger d_{002} values. Details about microstructure and magnetic properties are given in ref. [7].

3.3. Ribbons

Two kinds of ribbons (20 and 27 at% Cr) with thicknesses of 20–30 μm and widths of 6–10 mm were prepared by a spun-melt method. The exact compositions, measured by XRF were 19.8 and 27.2 at% Cr, repsectively. It was found from X-ray diffraction that both compositions were crystallised [38]. The M_s for the 20 and 27 at% Cr ribbon was 180 kA/m (which is much lower than the value of 228 kA/m expected from a random distribution) and 8 kA/m, respectively (which is close to the expected value for bulk material, namely zero).

4. Random distribution model of Co–Cr

The relation between the M_s vs. the at% Cr in Co can be represented by the Slater–Pauling curve [39]. In fig. 4 we used the data from Haines [40] to compare our experimental data. In the random Co–Cr alloy the Cr atoms are not distributed in the most suitable way for reducing the M_s of the alloy. Therefore the maximum local content of Cr for this distribution is much higher than in the case where Cr–Cr bonds are not present. The next line in fig. 4 shows the latter behaviour and it can be seen from this that the M_s becomes zero at 25 at% Cr based on the fact that for bulk material the measured M_s for this composition was zero. Consequently 4 Cr NN in a hcp lattice make the final M_s zero.

In the case of deposited Co–Cr films it is possible that a random distribution assembly of Cr atoms can be present in one area while in another area only a low concentration appears. For a given hcp structure of Co–Cr and a certain composition using the random distribution model one can calculate the frequency spectrum expected for spin-echo NMR based on a measured spectrum of a sputtered Co film (see fig. 5a). The spectra for 20 at% Cr (randomly distributed in the hcp Co) and 24 at% Cr are shown in figs. 5b and c, respectively. These results from a simulation program are obtained under the following assumptions:

1. The satellite peaks appear periodically in frequencies with a 40 MHz interval. This is qualitatively confirmed for the first and second satellite peaks by refs. [15,24] but not yet for the following peaks.
2. The main and satellite-peak frequencies change with the same concentration dependence.
3. All the resonance peaks (Gaussian shaped) have the same peak width and the same concentration dependence of each peak width.

For assumptions 2 and 3 the following should be mentioned: the satellite spectra have very complicated shapes as shown by ref. [15] because of the atomic configuration of non-magnetic nearest neighbours. The peak width for satellite peaks should be much broader than the main-peak width. Due to the fact that we do not have reliable data for the satellite-peak widths and the concentration dependencies we cannot incorporate these into our simulations. Another point is that at present we did not take into account the fact that the integral intensity of satellite peaks depends on the atomic configuration of non-magnetic NN as described by ref. [23]. Because our simulations are based on a very simple approach they can only be used, especially at the low frequency regions, as a rough estimation.

A very broad resonance peak containing the resonance lines of the various compositions available in a particular composition can be observed from the simulated data shown in figs. 5b and c. It can be seen that the peak shifts to lower frequencies when the amount of Cr increases.

If we now combine the same pure Co volume and 24 at% Cr (randomly distributed) then a spectrum as shown in fig. 6a appears. A composi-

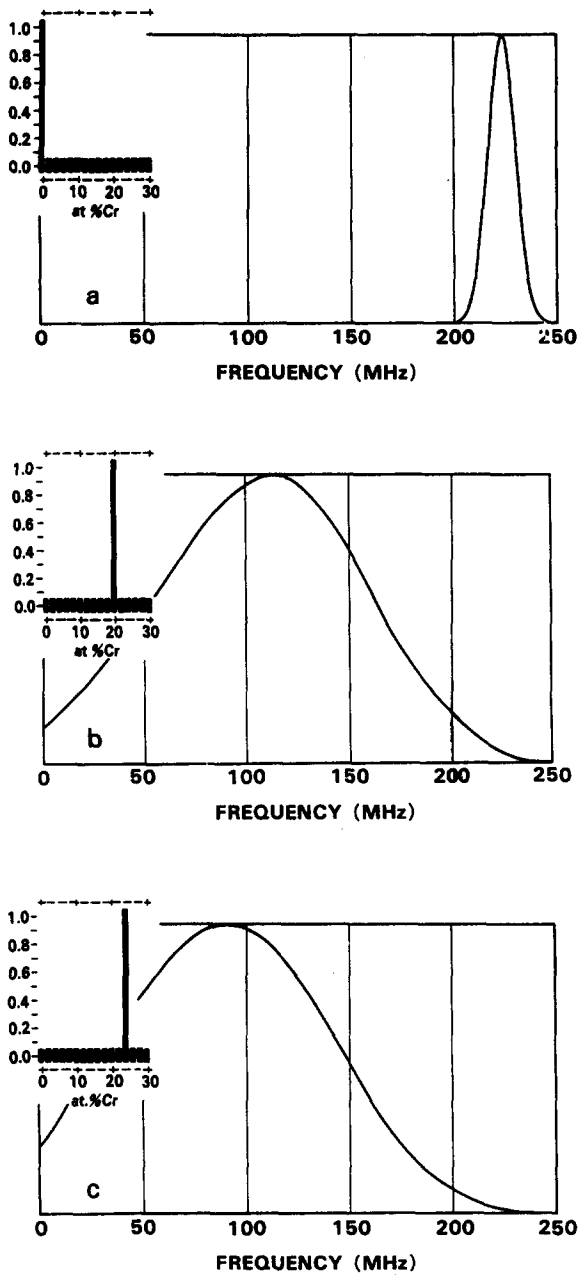

Fig. 5. Simulated NMR spectra for Co–Cr alloys based on a random distribution in a hcp structure from measured data of a sputtered Co film.

tional inhomogeneity partly consisting of pure Co and 4 compositions (2–8 at% Cr) and a larger part of randomly distributed 24 at% Cr is qualitatively given in fig. 6b. The main line is slightly decreased in frequency and the width is larger than the pure Co peak (see fig. 5a).

In fig. 6c a further simulation is given of a sample having a large volume of 8 at% Cr and a part with 28 at% Cr. If we change the large volume to a lower random composition, for instance, 2 at% Cr then fig. 6d is simulated. In this spectrum the main peak is closer to the pure Co and the intensity is again much higher in relation to the satellite(s).

Taking the above-mentioned comments about the simulations into account we still think that the presented simulations are very useful to obtain an idea about what can be expected in the various samples. Care must be taken when using them to explain exactly the composition of compositional distribution of the experimental data. There are too many sources that influence the actual samples which are not incorporated into the simulation program. For instance, experimentally, we always found lower intense satellite peaks than with the simulated spectra.

5. Experimental data of this study

We have measured a series of single-source Co–Cr samples having various compositions, 4 co-evaporated films with two thicknesses namely 400 and 700 nm prepared at room temperature (RT) and 400°C. As calibration samples we used two Co–Cr ribbons of 20 and 27 at% Cr and an evaporated Co-film.

The saturation magnetizations (M_s) of the samples are plotted in fig. 4 together with the lines calculated according to ref. [40]. It can be clearly seen that for all deposited films the M_s is higher than the random distribution line. Consequently they all are in an inhomogeneous state. The two ribbon samples have their magnetization under the random distribution line. It can be concluded from this that they have a more homogeneous composition. There is also a difference in magnetic properties between the co-evaporated and the single-source samples: M_s (at% Cr) is slightly larger while $H_{c\perp}$ is much larger for the co-evaporated samples.

For NMR measurements usually two samples of the same evaporation charge have been measured. In the case of co-evaporated samples NMR was carried out in two directions for two samples namely in the plane of evaporation and perpendicular to that plane. This was done to confirm the influence of the morphology on the NMR spectrum. It has been shown earlier [6,7] that the evaporation geometry causes different morphologies in both directions which consequently shown different magnetic properties. NMR measurements in both directions have shown no significant difference.

The magnetic properties of the samples are characterized by VSM and torque measurements. The average compositions have been determined by XRF.

5.1. Co–Cr ribbons and evaporated Co film

5.1.1. Co–Cr ribbons

Looking for an alternative calibration we prepared two Co–Cr ribbons containing an average composition of 20 and 27 at% Cr.

Simulations, for 20 and 28 at% Cr, based on the random distribution model have been carried out (see fig. 7). The 20 at% curve (fig. 7a) is based on 2 Cr NN and the 28 at% (fig. 7b) on 3 Cr NN. The NMR peak maximum for 28 at% Cr is about 67–70 MHz. On the contrary the 20 at% Cr shows its maximum at an even higher frequency namely 112–115 MHz. The peak width of the 27 at% Cr ribbon is smaller.

The experimental NMR spectra for both compositions are given in fig. 8. The main line fre-

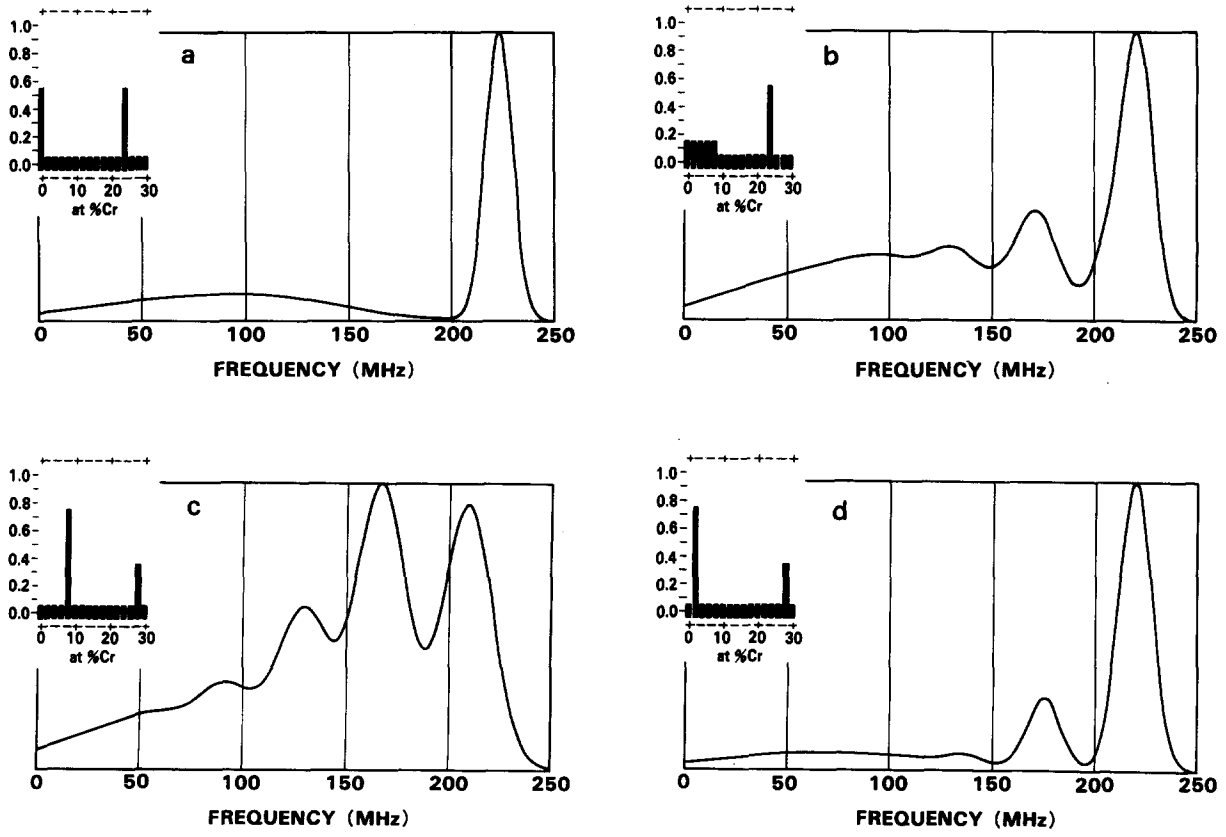

Fig. 6. Simulated spectra for compositional inhomogeneous Co–Cr samples.

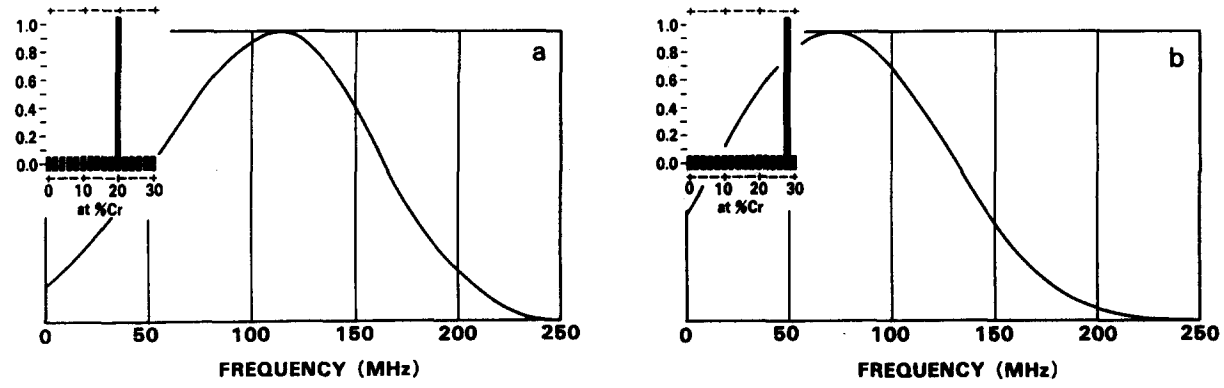

Fig. 7. Simulated spectra for a 20 and 28 at% Cr sample.

quency is about 35 MHz for both compositions but the peak width of 27 at% composition is smaller than for 20 at% Cr and shows a peak at 120 MHz coming from the sample holder (see later). In the case of the 20 at% Cr sample the main peak is too broad to detect the 120 MHz peak. The fact that the measured resonance frequency is much lower than the simulated one indicates that the ribbons have a much more homogeneous composition that a random distribution. Consequently they are closer to a distribution containing no Cr–Cr bonds. This is also supported by the low M_s values (see fig. 4). Measurements showed that the signal intensity for the 20 at% Cr sample is 7 times higher than for the 27 at% Cr. This is also mainly due to the fact that the M_s of the latter is nearly 0 at RT (8 kA/m) while the 20 at% sample has an M_s of 180 kA/m. It can be seen from the 20 at% Cr spectra that the peak is much sharper than those for powdered samples having a similar composition (see fig. 2). Besides this, the peak also shifts to a much lower frequency indicating a much more homogeneous contribution of the Cr in the Co.

5.1.2. Co film

A pure Co evaporated film has also been obliquely deposited ($\alpha_i = 27.5°$) and the NMR

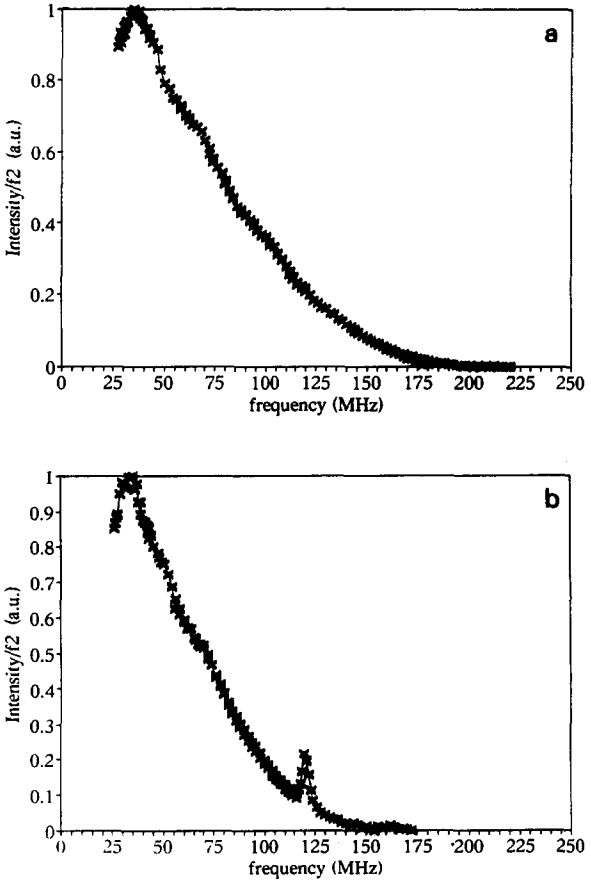

Fig. 8. Experimental NMR spectra of two Co–Cr ribbons. (a) 20 at% Cr and (b) 27 at% Cr.

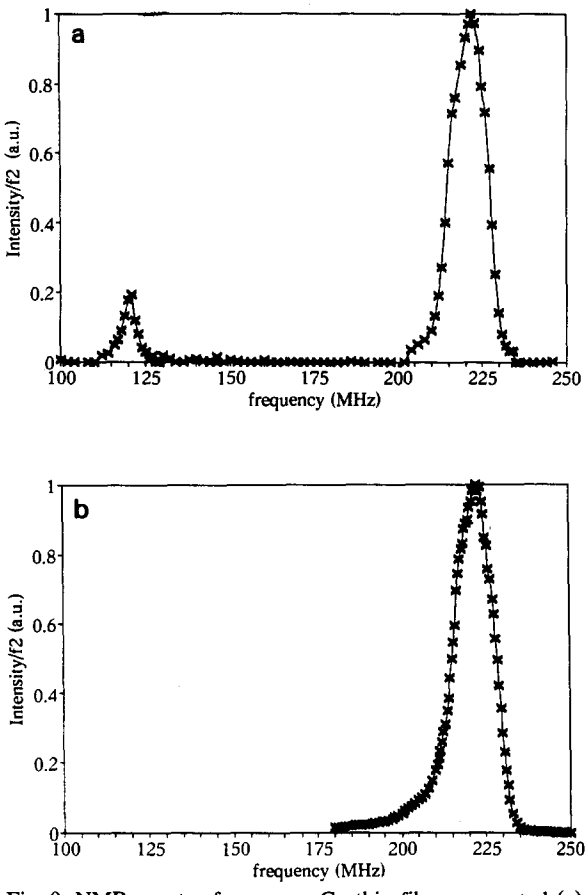

Fig. 9. NMR spectra for a pure Co thin film evaporated (a) and sputtered (b).

spectrum is given in fig. 9a. In comparison the data for a sputtered Co film by ref. [41] is also shown (fig. 9b). As can be seen there is nearly no difference between both types of films. Because the evaporated one has also been measured at low frequencies we can clearly observe the 120 MHz peak which is caused by Co in the plated Ni layers of the sample holder (refer also to section 5.4).

5.2. *Evaporated films with a single source*

The following can be concluded for the single-source films. Although all films show a compositional separation as indicated by the measured M_s value it should be realized that they have various stages of compositional separation. The very low M_s sample (high Cr content) only shows a broad spectrum without any echo frequency except at 120 MHz. The spectra for the other samples are given in fig. 10. Based on the average composition the 13.2% and the 18.6% sample

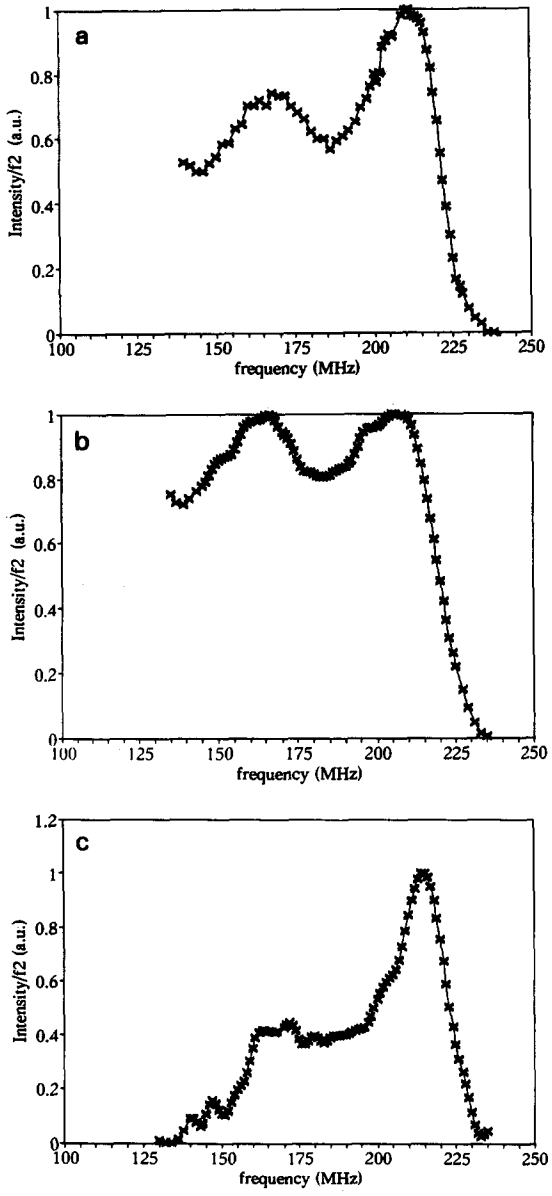

Fig. 10. NMR spectra of obliquely evaporated single source Co–Cr samples having various average compositions and made at RT and at 400 °C: (a) RT, 13.2 at% Cr; (b) RT, 18.6 at% Cr; (c) 400 °C, 26.6 at% Cr.

show a trend from which the frequency shift of the main and satellite peaks can be explained as follows. With increasing Cr content the resonance frequency of the main line decreases and the width of the peak increases. Further the first satellite peak increases its intensity with respect to the main line.

The first satellite of the high temperature sample is small and the frequency of the main line is higher than for the ambient temperature samples. This indicates that its state is less homogeneous and the amount of Cr in the Co-rich ferromagnetic area is less. Of course, due to the higher deposition temperature (400°C), it was already expected to have the highest compositionally separated state (see also table 3). This fact is also supported by the highest $H_{c\perp}$ which is caused by more pinning sites of the domain wall or a combination of domain-wall motion and rotation.

5.3. *Co-evaporated samples*

Fig. 11 shows the 4 NMR spectra for the co-evaporated Co–Cr samples having thicknesses of 400 and 700 nm prepared at RT and 400°C.

All samples (thick and thin) show the main peak at a frequency between 223 (RT) and 217 MHz (high temperature) which means that they have a very inhomogeneous composition with almost pure Co-regions. Comparing the ambient (RT) and high-temperature (HT) samples we came to the conclusion that the latter has more inhomogeneity (higher hyperfine field).

Based on NMR main-line frequency Yoshida et al. [37] introduced a method to calculate the ferromagnetic and less-ferromagnetic part. For this estimation the average Cr content and the M_s as function of the Cr content should also be known. The average Cr content C_{av} can be determined by XRF and is given by $C_{av} = C_f V_f + C_l V_l$, in which C_f and C_l are the local Cr concentrations of the ferromagnetic and less-ferromagnetic regions. In this terminology the ferromagnetic volumepart concerns a Co-rich component without any Cr atoms among the next neighbours of Co. The concentration C_f is taken from the NMR data for powder Co–Cr and M_s (at% Cr) as well.

The sum of the volumes of both regions ($V_f + V_l$) is one. The M_s of the whole film, measured by VSM is in fact the product of $M_s \times V_f$ (here M_s is the local saturation magnetization of the ferromagnetic region on the Cr concentration). Table 3 gives the results for RT and HT Co–Cr samples. All data show a Co-rich component. The volume part of this component is larger for the high temperature samples than for the room-temperature ones. Consequently a higher compositionally separated state occurs in the HT samples. Looking to the C_f data from table 3 it can be clearly concluded that this value is lower for RT as for HT co-evaporated values. The latter is smaller than the C_f values in the single source

Table 3
Volumetric ratio of ferro and non-ferromagnetic regions

Sample	Film thickness [nm]	at% Cr (XRF)	NMR local at% Cr		Calculated volume ratio	
			C_f	C_l	V_f	V_l
RT co-evaporated	356	24.7	3.0	36.9	0.36	0.64
	648	21.5	2.5	33.6	0.39	0.61
HT co-evaporated	399	27.6	5.9	42.1	0.40	0.60
	753	27.3	5.3	43.2	0.42	0.58
RT one source	186	13.2	9.1	30.7	0.81	0.19
	227	18.6	11.6	39.6	0.75	0.25
HT one source	207	26.6	7.4	42.3	0.45	0.55

C_f: concentration of Co-rich component without any Cr atoms among the next neighbours of Co.
C_l: concentration of less-ferromagnetic components.
V_f: volume ratio of Co-rich component without any Cr atoms among the next neighbours of Co.
V_l: volume ratio of less-ferromagnetic components.

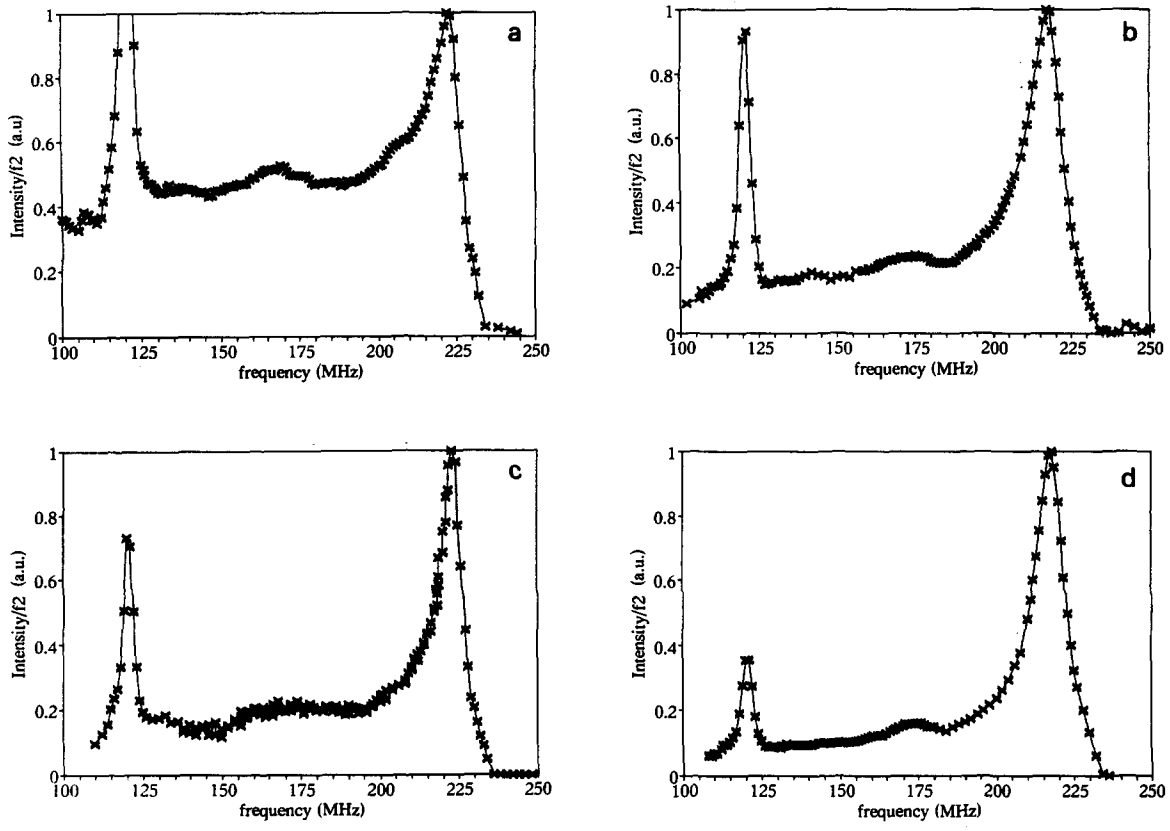

Fig. 11. NMR spectra of 4 co-evaporated Co–Cr films. (a) RT, 356 nm; (b) 400 ° C, 399 nm; (c) RT, 648 nm; (d) 400 ° C, 753 nm.

samples. The data from the ferromagnetic region clearly proves the existence of process-induced compositional separation. Furthermore it is interesting to mention that the $H_{c\perp}$ of the single source samples (see table 1) are lower than those for the co-evaporated ones. But we have to keep in mind that at% and film thicknesses are not the same in both type of samples.

5.4. The 120 MHz peak

All spectra discussed, including the ribbons and pure Co film, show a sharp peak at about 120 MHz. It was recently found that this peak originated from a material component of the sample holder.

6. Conclusions

1. Independent of the preparation technique deposited Co–Cr films have shown a main-line and satellite line(s) which can be interpreted as inhomogeneous compositions. In single source evaporated samples a high temperature is needed for evaporated better magnetic properties, i.e. higher coercivity. It has been shown for co-evaporated films that even at room temperature this stage can be reached.
2. Using VSM, XRF and NMR data we have shown that in our co-evaporated films deposited at room temperature a compositional separation occurs which we call a process-induced compositional separation.

3. The volume part of the Co-rich component increases with deposition temperature for the co-evaporated samples. There is a decrease of this volume part for the single-source samples which is caused by the very high Cr content of the high temperature sample.
4. The Co–Cr ribbons used in this study are better for calibration than the powdered samples that have been used up to now. They appear to be more homogeneous than the powder samples.
5. The evaporated pure Co sample shows a frequency of the main line which can be compared with the literature data of bulk Co samples. Furthermore there is no significant difference between evaporated and sputtered Co films.

Acknowledgement

The first author appreciated the invitation and financial support from NTT for a two-month stay at the NTT Basic Research Laboratories, Material Science Research Laboratory, Tokai, Japan.

References

[1] S. Iwasaki and K. Takemura, IEEE Trans. Magn. MAG-11 (1975) 1173.
[2] See for example Proc. Second PMRC'91, 8–11 October 1991, Hachimantai, Iwate, Japan (1991).
[3] R.M. Bozorth, Ferromagnetism (Van Nostrand, New York, 1951) p. 441.
[4] F.A. Pronk and J.C. Lodder, IEEE Trans. Magn. MAG-24 (1988) 1744.
[5] F.A. Pronk and J.C. Lodder, J. de Phys. 49 (1988) C8-1991.
[6] H. v. Kranenburg, J.C. Lodder, Y. Maeda, L. Toth and Th.J.A. Popma, IEEE Trans. Magn. MAG-26 (1990) 1620.
[7] H. v. Kranenburg, J.C. Lodder, Th.A.J. Popma, K. Takei and Y. Maeda, J. Magn. Soc. Jpn. 15 Suppl. S2 (1991) 33.
[8] Y. Maeda, S. Hirono and M. Asahi, Jpn. J. Appl. Phys. 24 (1985) L951.
[9] Y. Maeda, M. Asahi and M. Seki, Jpn. J. Appl. Phys. 25 (1986) L668.
[10] Y. Maeda and M. Asahi, J. Appl. Phys. 61 (1987) 1972.
[11] H. Masuya and H. Awano, IEEE Trans. Magn. MAG-23 (1987) 2064.
[12] Y. Maeda and M. Takahashi, IEEE Trans. Magn. MAG-24 (1988) 3012.
[13] K. Takei and Y. Maeda, Jpn. J. Appl. Phys. 30 (1991) L1125.
[14] K. Yoshida, K. Imagawa, F. Kugiya, H. Daimon, S. Yamagata, O. Kitakami and H. Yasuoka, J. Magn. Soc. Jpn. 13 Suppl. S1 (1989) 425.
[15] K. Yoshida, H. Kakibayashi and H. Yasuoka, J. Appl. Phys. 68 (1990) 705.
[16] W. Pauli, Naturwisschenschaften 12 (1924) 741.
[17] W. Marshall, Phys. Rev. 110 (1958) 1280.
[18] A.M. Portis and R.H. Lindquist, in: Magnetism, vol. II, part A, eds. G.T. Rado and H. Suhl (Academic Press, New York, 1965) p. 357.
[19] R.F. Jackson, R.G. Scurlock, D.B. Utton and T.H. Wilmhurst, Proc. Intern. Conf. Magnetism, Nottingham (1964) p. 384.
[20] M. Kawakami, J. Phys. Soc. Jpn. 40 (1976) 56.
[21] The apparatus was developed by Drs. Y. Maeda and K. Takei of the NTT Basic Research Laboratories, Material Science Research Laboratory, Tokai, Ibaraki, Japan.
[22] J.I. Budnik and S. Skalski, in: Hyperfine Interactions, eds. A.J. Freeman and R.B. Frankel (Academic Press, New York, 1967) p. 724.
[23] S. Nasu, H. Yasuoka, Y. Nakamura and Y. Murakami, Acta Mellurgica 22 (1974) 1057.
[24] S.I. Kobayashi, K. Asayama and J. Itoh, J. Phys. Soc. Jpn. 21 (1966) 65.
[25] Murry and Marshall, Proc. Intern. Conf. on Magnetism (1964) p. 387.
[26] Y. Koi, A. Tsujimura, T. Hihara and T. Kushida, J. Phys. Soc. Jpn. 17 Supp. B-I (1962) 96.
[27] R.C. LaForce, S.F. Ravitz and G.F. Day, Phys. Rev. Lett. 6 (1961) 226.
[28] W.A. Hardy, J. Appl. Phys. 32 Suppl. 3 (1966) 122S.
[29] S. Nasu, H. Yasuoka, Y. Nakamura and Y. Murakami, Acta Metallurgica 19 (1971) 561.
[30] R. Street, D.S. Rodbell and W.L. Roth, Phys. Rev. 121 (1961) 84.
[31] D.A. Anderson and G.A. Smart, J. Appl. Phys. 35 (1964) 3043.
[32] A.R. Elsea, A.B. Westerman and G.K. Manning, Trans. AIME 180 (1949) 579.
[33] A.T. Grgor'ev, E. Yu-p'u and E.M. Sokolovskaya, Russ. J. Inorg. Chem. 6 (1961) 827.
[34] C. Allibert, C. Bernard, N. Valignat and M. Dombre, J. Less-Common Met. 59 (1978) 211.
[35] K. Ishida and T. Nishizawa, Bull. Alloy Phase Diag. 11 (1990) 357.
[36] B. Chapman, Glow Discharge Sputtering (John Wiley. New York, 1990) p. 199.
[37] K. Yoshida, H. Kakibayashi and H. Yasuoka, Mater. Soc. Symp. Proc. 232 (1991) 47.
[38] Ning Zhang and J.C. Lodder, J. Magn. Magn. Mater. 89 (1990) 284.
[39] J.C. Slater, J. Appl. Phys. 8 (1937) 385.
L. Paulîng, Phys. Rev. 54 (1938) 899.
[40] W.G. Haines, J. Appl. Phys. 55 (1984) 2263.
[41] Measured by Dr. Takei and Dr. Maeda, unpublished data.